JACS
JOURNAL OF THE AMERICAN CHEMICAL SOCIETY
Article
pubs.acs.org/JACS

Photoinduced C–C Reactions on Insulators toward Photolithography of Graphene Nanoarchitectures

Carlos-Andres Palma,*[,†] Katharina Diller,[†] Reinhard Berger,[‡] Alexander Welle,[§] Jonas Björk,[∥] Jose Luis Cabellos,[⊥] Duncan J. Mowbray,[⊥] Anthoula C. Papageorgiou,[†] Natalia P. Ivleva,[¶] Sonja Matich,[□] Emanuela Margapoti,[□] Reinhard Niessner,[¶] Bernhard Menges,[‡] Joachim Reichert,[†] Xinliang Feng,[‡] Hans Joachim Räder,[‡] Florian Klappenberger,*[,†] Angel Rubio,*[,⊥,#] Klaus Müllen,*[,‡] and Johannes V. Barth[†]

[†]Physik-Department, Technische Universität München, James-Franck-Strasse 1, 85748 Garching, Germany

[‡]Max-Planck-Institut für Polymerforschung, Ackermannweg 10, 55128 Mainz, Germany

[§]Institut für Funktionelle Grenzflächen, Karlsruher Institut für Technologie, Hermann-von-Helmholz-Platz 1, 76344 Eggenstein-Leopoldshafen, Germany

[∥]Department of Physics, Chemistry and Biology, IFM, Linköping University, 58183 Linköping , Sweden

[⊥]Nano-Bio Spectroscopy Group and ETSF Scientific Development Centre, Departamento de Física de Materiales, Centro de Física de Materiales CSIC-UPV/EHU-MPC DIPC, Universidad del País Vasco UPV/EHU, Av. Tolosa 72, E-20018 San Sebastián, Spain

[¶]Chair for Analytical Chemistry, Institute of Hydrochemistry, Technische Universität München, Marchioninistr. 17, 81377 München, Germany

[□]Walter Schottky Institut and Physik-Department, Technische Universität München, Am Coulombwall 4a, 85748 Garching, Germany

[#]Fritz-Haber-Institut Max-Planck-Gesellschaft, Berlin, Germany

Supporting Information

ABSTRACT: On-surface chemistry for atomically precise sp^2 macromolecules requires top-down lithographic methods on insulating surfaces in order to pattern the long-range complex architectures needed by the semiconductor industry. Here, we fabricate sp^2-carbon nanometer-thin films on insulators and under ultrahigh vacuum (UHV) conditions from photocoupled brominated precursors. We reveal that covalent coupling is initiated by C–Br bond cleavage through photon energies exceeding 4.4 eV, as monitored by laser desorption ionization (LDI) mass spectrometry (MS) and X-ray photoelectron spectroscopy (XPS). Density functional theory (DFT) gives insight into the mechanisms of C–Br scission and C–C coupling processes. Further, unreacted material can be sublimed and the coupled sp^2-carbon precursors can be graphitized by e-beam treatment at 500 °C, demonstrating promising applications in photolithography of graphene nanoarchitectures. Our results present UV-induced reactions on insulators for the formation of all sp^2-carbon architectures, thereby converging top-down lithography and bottom-up on-surface chemistry into technology.

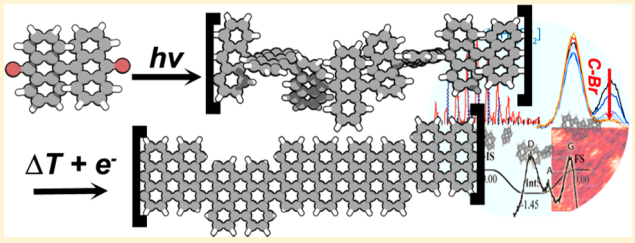

INTRODUCTION

On-surface engineering of covalent sp^2 architectures[1,2] is a growing discipline that strongly relies on scanning probe characterization on well-defined surfaces. Today a hand-full of molecular and atomically precise materials[3−5] have been fabricated by exploiting thermomolecular reactions occurring mostly at metallic interfaces. Just recently, molecular materials of technological importance belonging to the family of graphene nanoribbons have been synthesized by the C–Br dissociation and aryl–aryl coupling of a brominated precursor on Au(111) followed by dehydrogenation at 400 °C[4] for graphitization.[6] Using well-defined single-crystal playgrounds, most on-surface synthesis work has been carried out on low-index metallic surfaces[5,7] as a catalytic requirement for C–C coupling. The alternate approach of using nonmetallic substrates has been rarely investigated.[8,9] More importantly, the aforementioned on-surface reactions occur in 2D confinement with reduced dimensionality. Thus, the thermomolecular reaction conditions are highly dependent on diffusion of the precursors on the surface.[10] The colossal task simultaneously predicting the structure chemistry and the final absolute spatial orientation of a molecular structure, represents a major obstacle for the transition of on-surface chemistry into technology. Such

Received: December 18, 2013
Published: February 13, 2014

   dx.doi.org/10.1021/ja412868w | J. Am. Chem. Soc. 2014, 136, 4651−4658

Scheme 1. Coupling Reaction Intermediates and Graphitization[a]

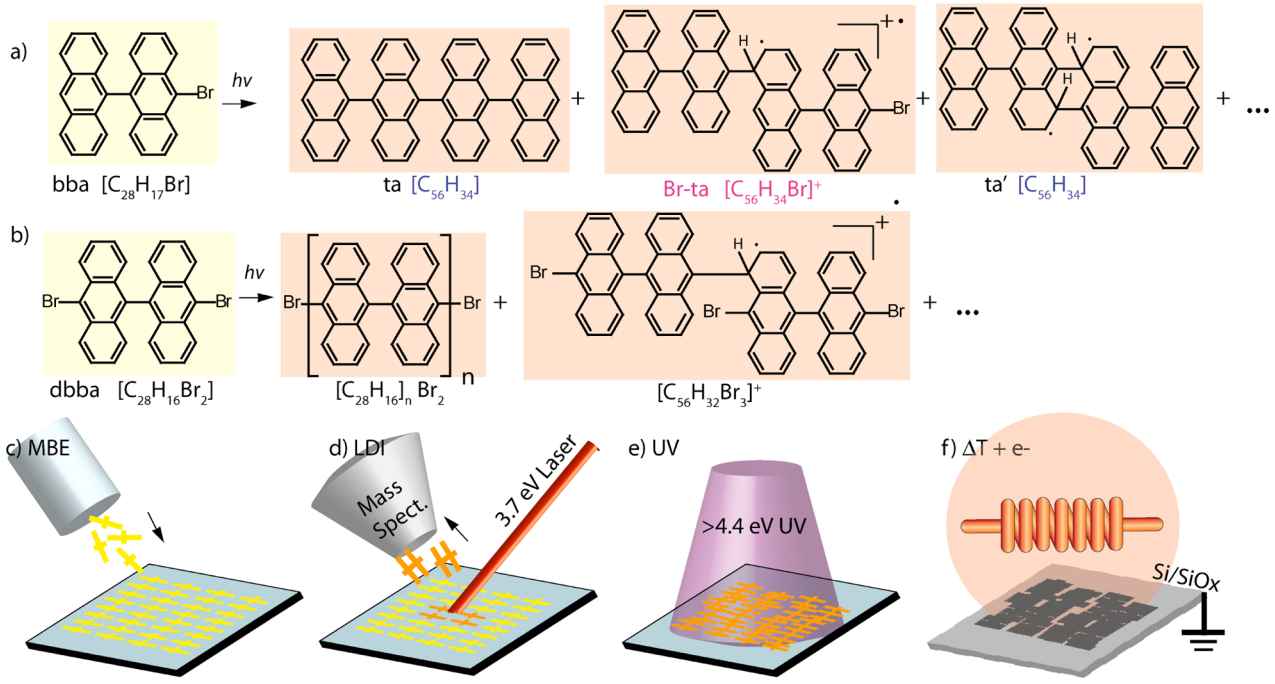

[a](a) Upon UV irradiation in nanometer-thin films under UHV conditions, 10-bromo-9,9′-bianthryl (**bba**, 432 g·mol^{-1}) can react producing 9,10-tetraanthrylene, (**ta**, 706 g·mol^{-1}), **Br-ta** (786 g·mol^{-1}) or the **ta** isomer (**ta**′), among others. (b) 10,10′-dibromo-9,9′-bianthryl (**dbba**, 510 g·mol^{-1}) undergoing analogous UV-induced reactions. (c–f) General procedure: (c) molecular beam epitaxy (MBE) of precursor multilayers (**bba** or **dbba**) on a mica or silicon oxide/silicon wafer, (d) monitoring UV reactions via laser desorption ionization (LDI) mass spectrometry. (e) UV irradiation of multilayers and (f) e-beam annealing treatment of multilayers. Yellow and orange drawings refer to the molecular structures in (a) and (b).

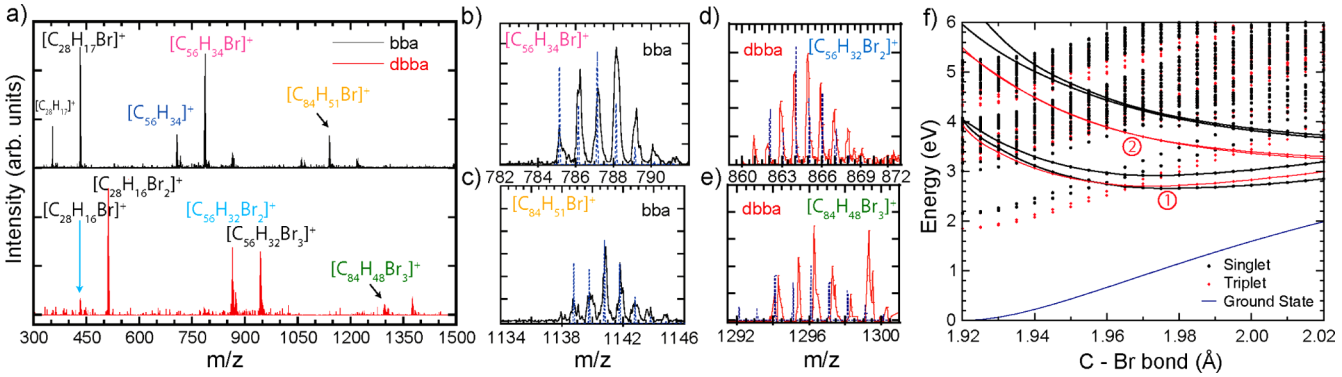

Figure 1. Photoinduced C–C coupling reaction intermediates via direct laser desorption ionization. (a) LDI MS-ToF spectra for **bba** with (black) and **dbba** (red) at 20 mJ cm^{-2} irradiation power using a 3.7 eV (337 nm) nanosecond-pulsed laser. (b) Detail of the **bba** $[C_{56}H_{34}Br]^+$ region showing the **Br-ta** structure in Scheme 1. (c) Detail of the **bba** $[C_{84}H_{51}Br]^+$ region. (d) Detail of the **dbba** n = 2 oligomer $[C_{56}H_{32}Br_2]^+$ region and (e) the **dbba** n = 3 oligomer region showing a tribrominated adduct $[C_{84}H_{48}Br_3]^+$. Simulated isotopic distributions are shown in blue dotted lines in (b–e). (f) TD-DFT calculated C–Br dissociation adiabatic pathways for **dbba**, where 1.92 Å is the equilibrium distance. Dissociation channels (1) and (2) can be (indirectly) excited 3.7 and 4.4 eV, respectively, at a C–Br bond distance of 1.96 eV.

control is essential for the fabrication of large-area carbon sp^2 circuits.[2] To simplify this challenge, the semiconductor industry requires a top-down approach for directly patterning on-surface chemistry products. One alternative is to photochemically process tightly packed mono- or multilayers directly[2,11] and to subsequently remove unreacted material. Here we show that photoreacting nanometer-thin films of dibromo-bianthryls on insulators produce coupled sp^2-carbon multilayers from C–C coupling reaction intermediates (Scheme 1a,b). After UV irradiation of the evaporated material on mica substrates, the coupled sp^2-carbon multilayers can be dehydrogenated, i.e. graphitized, at as low as 500 °C using e-beam irradiation, thus opening up technological applications (Scheme 1c,f). The studies present the formation of the coupled multilayers both as a concerted and a two-step process, undergoing C–Br photodissociation and C–C coupling. The use of filtered UV light in conjunction with time-dependent density functional theory (TD-DFT) calculations suggests that the dissociation mechanism is occurring through resonant excitation and subsequent intersystem crossing to a repulsive triplet state. Unlike UV-induced reactions of multilayers, X-ray photoelectron spectroscopy reveals how thermal treatment of the multilayers alone results in almost complete loss (desorption) of the material, presenting coupled sp^2-carbon multilayers as

dx.doi.org/10.1021/ja412868w | J. Am. Chem. Soc. 2014, 136, 4651–4658

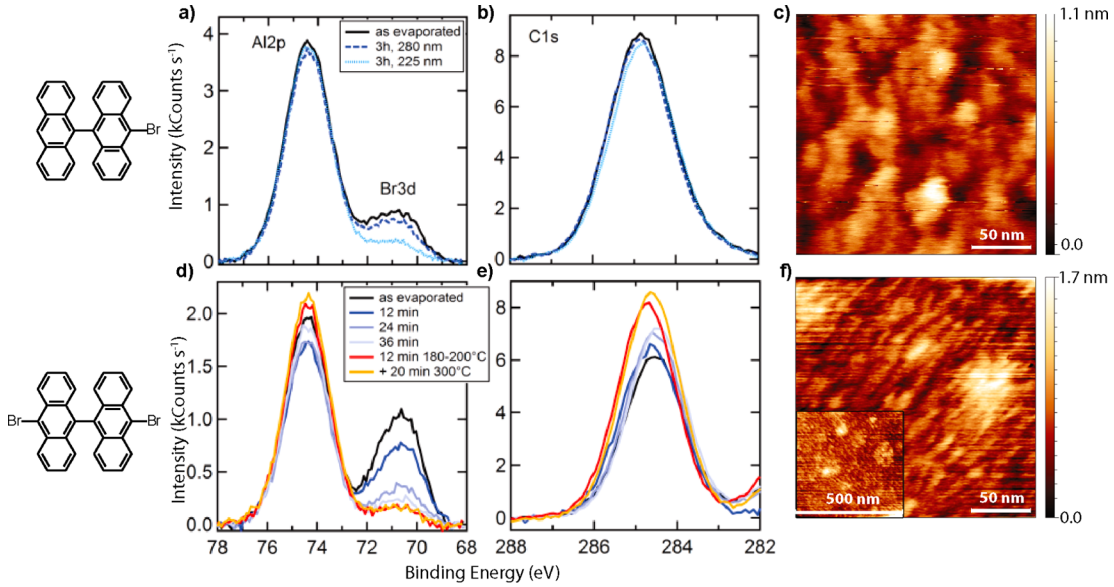

Figure 2. Monitoring C−Br photodissociation and sp^2-carbon signal through X-ray photoelectron spectroscopy. (a,b) The XPS measurements of UV-irradiated **bba** nanometer-thin films using two different filters indicate that wavelengths between 280 and 225 nm are responsible for C−Br dissociation. (d,e) UV-irradiated **dbba** (no filter). (c,f) Atomic force microscopy imaging of the respective samples to the l.h.s. showing the last preparation step: for (c) **bba** and (f) **dbba** multilayers after UV irradiation and flash annealing. The inset in (f) shows a 500 × 500 nm^2 survey.

technologically important photoresists. Subsequent annealing of UV-irradiated multilayers results in detection of long, nanometer-wide sp^2-carbon nanoarchitectures in the film morphology and graphitization, revealed by atomic force microscopy (AFM) and Raman spectroscopy, respectively. Finally, we give perspectives toward atomically precise fabrication in nanometer-thin films on insulating substrates.

RESULTS AND DISCUSSION

The photodissociation of aryl halides is a well-known process,[12] much less is known about the mechanism and reactivity of photogenerated aryl radicals toward highly selective polymerization reactions.[9,13] Time-of-flight (ToF) laser desorption ionization (LDI, using a 3.7 eV nitrogen laser) mass spectrometry (MS) provides a state-of-the-art nanochemistry method for identifying both photodissociation and C−C coupling intermediate structural isomers. Figure 1a−e shows the MS at positive ion detection for the LDI powder samples of **bba** and **dbba**. The peaks at higher masses are indications of newly formed C−C bonds following the suggested reaction products in Scheme 1a,b. For **bba** (Figure 1a black line) the debrominated precursor, $[C_{28}H_{17}]^+$ observed at 354 m/z, is a clear indication of C−Br dissociation. Then, the two carbon isotropic distributions starting at 705 and 707 m/z (Figure 1a, blue $[C_{56}H_{34}]^+$) can be attributed to the structures **ta**, **ta**′ and their isomers. The main product of the **bba** LDI appears between 785 and 786 m/z (Figure 1a,b black line) and is assigned to **Br-ta** $[C_{56}H_{34}Br]^+$ (Scheme 1, in magenta). This is the first indication that nonselective photoinduced reactions can occur, that is, reactions not leading to a well-defined desired **ta** isomer. The unexpected observation of **bba** trimers $[C_{84}H_{51}Br]^+$ which are detected at 1138 m/z (Figure 1a,c in yellow), confirms such nonselective reactions. The intensity of the debrominated **bba** peak suggests that the radical yield in LDI experiments is close to 40%. However, considering $[C_{28}H_{17}]^+$ as a radical intermediate for all reactions and an homogeneous ionization process, summing all the reacted species (dimers, trimers, etc.) yields 70% C−Br dissociation efficiency at laser powers of 20 mJ cm^{-2}. For the dibromo precursor, **dbba**, the peaks of the LDI spectra at 862 m/z are a clear indication of the formation of an n = 2 oligomer $[C_{56}H_{32}Br_2]^+$ (Figure 1a,d red line). Here also the n = 3 oligomer $[C_{84}H_{48}Br_3]^+$ is detected. Again for **dbba** nonselective oligomerization reactions occur, as demonstrated by the formation of side products, mainly triple brominated n = 2 adduct $[C_{56}H_{32}Br_3]^+$ at exactly 941 m/z (Figure 1a,e in green). Such a triple brominated product is attributed to a structure as depicted in the right panel of Scheme 1b. Also for **dbba**, the C−Br scission product $[C_{28}H_{16}Br]^+$ is observed at 431 m/z. Note that oligomers are not observed when using a 7,7,8,8-tetracyanoquinodimethane (TCNQ) matrix in conjuction with **dbba** or **bba**, in the analogous matrix-assisted laser desorption ionization (MALDI) technique. Moreover, we emphasize that the LDI of the pristine 9′9-bianthracene compound ($C_{28}H_{18}$) does not show the presence of oligomers. This excludes dimerization through alternative well-known anthracenic [4 + 4] photocyclization[14] mechanisms with such bulky precursors and under our conditions (Figure S1a in SI). It is worth noting that LDI also provokes oligomerization in solid-state powders of brominated pyrene compounds and other species (see Figures S1b and S2 in SI).

To study the C−Br scission process from first principles, we performed TD-DFT calculations on the dissociation of the C−Br bond in **dbba**. We made use of an excitation matrix overlap approach (see SI) to find adiabatic reaction pathways along the singlet and triplet excitations. Although relatively inexpensive computationally, our level of theory shows excellent agreement with reported[15] quantum chemical calculations on the dissociation of bromobenzene (first singlet and triplet non-dissociative adiabatic channels appear at 4.8 and 4.0 eV, respectively, in our calculations and 4.7 and 4.0, respectively, in the diabatics of Liu et al.,[15] see Figure S3 in SI for the full bromobenzene adiabatic pathway). Figure 1f shows the adiabatic reaction pathways for **dbba** along the C−Br reaction coordinate, starting at the ground state C−Br bond length of

dx.doi.org/10.1021/ja412868w | J. Am. Chem. Soc. 2014, 136, 4651−4658

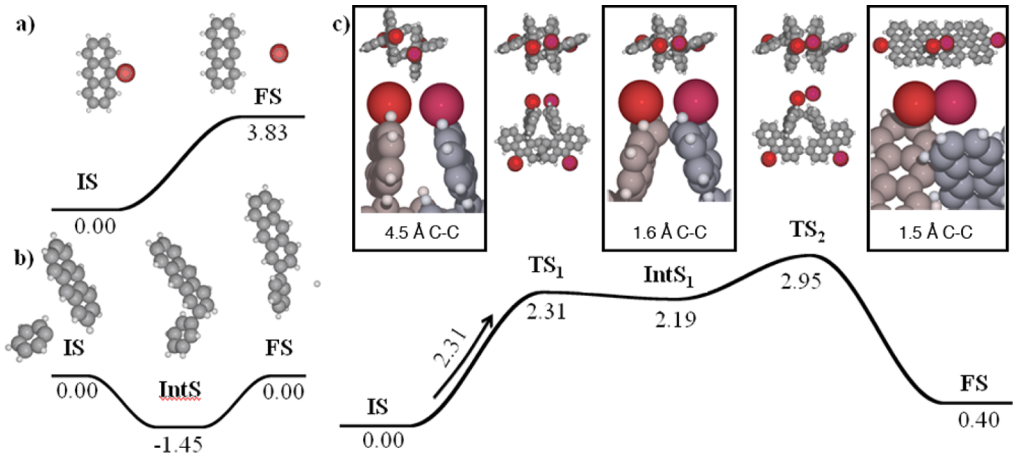

Figure 3. DFT insight into C−Br dissociation C−C coupling mechanisms. (a) Heterolytic C−Br dissociation in vacuum produces a radical pair with 3.8 eV in energy. (b) The spontaneous reaction of an aryl-radical with anthracene and subsequent dehydrogenation has the same activation barrier. (c) A face-on concerted dissociation−coupling bimolecular mechanism showing C−C coupling in an intermediate state ($IntS_1$) and subsequent C−Br dissociation. The path features a lower activation energy than the heterolytic dissociation in (a) by 0.9 eV. C, Br, and H atoms are depicted by gray, red, and white, respectively.

1.92 Å. The first (1) pair of triplet and singlet (Figure 1f red and black lines, respectively) dissociation channels cross the vertically excited ground state (Figure 1f, dotted lines) close to 4.0 eV (310 nm). These channels involve transitions from the anthracene π orbitals to the opposite (lower energy) or adjacent (higher energy) antibonding C−Br σ^* orbital. For a C−Br bond stretching of 0.05 Å, which is consistent with the temperatures studied, the vertical excitation energy is approximately 3.7 eV. This suggests the (1) singlet channels are responsible for the observed C−Br dissociation in the LDI experiments. However, since the probability of an excitation to (1) is rather low when **dbba** is exposed to a filtered UV lamp, we observe C−Br dissociation only for energies above 4.4 eV (*vide infra*). This is consistent with excitation to one of the singlet attractive channels between 4.4 and 5.5 eV, followed by an intersystem crossing to a second (2) pair of repulsive triplet channels 5.5 eV (225 nm). These (2) triplet channels involve transitions from the $2p_y$ or $2p_z$ states of the Br to the antibonding C−Br σ^* orbital. This second dissociation channel is also in agreement with bromoanthracene photophysics experiments, which identify such high-lying triplets as the main C−Br dissociation channels.[16] Both orbitals are present in the dibrominated single anthracene (**dba**, Figure S2d in SI), and thus the dissociation channels in **dba** and **dbba** are similar.

To provide evidence for the main photodissociation channel behind C−Br photodissociation, we use XPS to examine the C−Br scission under two different light-irradiation conditions and sources. The UHV-prepared multilayer films of **dbba** (as used in the LDI experiments) and the model system **bba** were investigated (see Experimental Section). Figure 2a,b shows the Br3d (a) and C1s (b) spectra of the **bba** multilayer. In the Br3d region of the pristine **bba** (Figure 2a continuous black line) two peaks are discernible: the Al2p line of the mica substrate which was used as a reference for the calibration of the energy scale (see Experimental Section and SI) and the Br3d line of the **bba** molecules. Both peaks consist of a doublet, whose small energy splitting does not allow them to be resolved separately due to the limited resolution of the experimental setup. For the chosen energy reference the fitting of the Br3d peaks results in binding energies of $Br3d_{5/2}$ = 70.6 eV and $Br3d_{3/2}$ = 71.7 eV. These values are typical for Br in a covalent bond with carbon[17] and similar to those for bromobenzene[18] and exclude their assignment to neutral bromine ($Br^0 3d_{5/2}$ = 69 eV[19]). In combination with the cross-section-corrected[20] C1s/Br3d area ratio, this indicates that intact molecular layers are obtained with our preparation routine. The C1s region (Figure 2b continuous black line) exhibits one single peak at 284.8 eV. As opposed to the LDI experiments, no change in the XP spectra could be observed for the samples irradiated by a 3.7 eV pulser laser (4 ± 1 mW cm^{-2} irradiation). Note that the same (but unfocused) laser source as in the LDI experiments was used. This observation points toward the previous LDI photodissociation experiments being either thermally assisted (because of high temperatures in the matrix-assisted LDI plume[21]) or due to high fields during the ionization process, in agreement with the previous TD-DFT discussion. With this in mind, low-pass filters were installed in conjunction with a 120-W high-pressure mercury lamp (nominal irradiation 58 ± 10 mW cm^{-2} at 15.1 cm sample distance) in order to identify other possible C−Br dissociation channels. Irradiating the **bba** samples for 180 min using glass filters with 0.01 transmittance above 345, 335, 320, 295, and 280 nm leads only to small changes in the Br3d and C1s signals (Figure 2a,b dark-blue lines and Figure S9a in SI). If, however, a filter blocking wavelengths exclusively below 225 nm (transmitting up to 5.5 eV energies) is used, the Br3d peak decreases considerably with only negligible effects on the C1s signal (Figure 2a,b light-blue lines). This indicates that a scission of the C−Br bond and a subsequent desorption of Br occurs. Such a decrease is equal to that found using unfiltered UV light (see Figure S4 in SI). The previous filter studies situate the dissociation channel between 4.4 and 5.5 eV, indicating that an intersystem crossing to the second (2) triplet repulsive adiabatic (red line, Figure 1f) is behind the main dissociation channel for both **dbba** and **bba** in UV experiments (orange line, Figure 1f).

For **dbba**, Figure 2d,e illustrates the changes of the XP spectra upon UV irradiation (without filter), followed by thermal treatment. As was the case for **bba**, the amount of Br is reduced after UV irradiation. Interestingly, the C−Br scission reaches a stationary point. A constant Br3d peak height is reached for both **bba** and **dbba**, after which the UV irradiation is no longer effective. After this point the Br3d peak can be

dx.doi.org/10.1021/ja412868w | J. Am. Chem. Soc. 2014, 136, 4651−4658

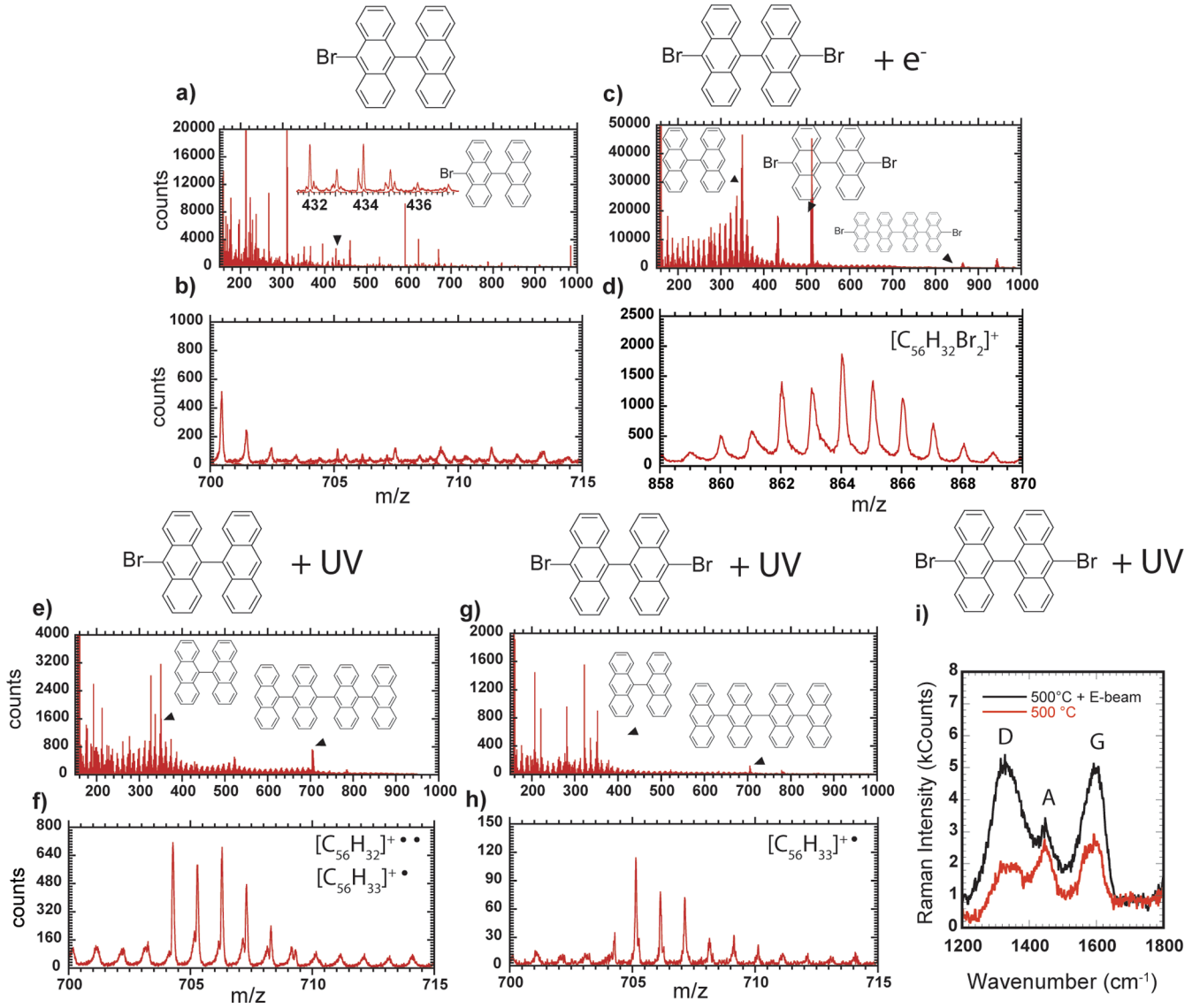

Figure 4. Detection of coupled intermediates and Raman spectroscopy of graphitized multilayers. ToF-SIMS of **dbba** and **bba** multilayers. (a,b) Pristine **bba** drop-casted on gold. (c,d) MBE **dbba** multilayers on muscovite mica. On insulating muscovite mica, a 21 eV electron flood-gun must be used to compensate for surface charging during SIMS, producing electron-induced brominated dimers. (e,f) UV-irradiated **bba** multilayers showing the main dimer $[C_{56}H_{32}]^+$ signal. (g,h) UV-irradiated **dbba** multilayers also showing the main dimer $[C_{56}H_{32}]^+$ signal. Multilayers in (e–h) were flash annealed at 300 °C to remove any remaining bromine and unequivocally avoid false positive brominated dimers signals. (i) Raman spectra (λ_0 = 532 nm) of the UV-irradiated multilayer on SiO_x/Si wafer after annealing at 500 °C with and without direct e-beam heating. A broad D mode is shown centered at 1330 cm^{-1}, while the G mode is centered at 1595 cm^{-1}. The A mode corresponds to the Raman active signal of the UV-irradiated multilayer at 1445 cm^{-1}.

further reduced by flash annealing to 300 °C (red and orange curves in Figure 2d,e). Here the C1s signal remains constant or even increases, i.e., the decrease in the Br3d signal is not related to desorption of the molecular species. In fact, when annealing **dbba** multilayers (i.e., without UV irradiation), almost complete disappearance of both C1s and Br3d peaks is observed (See Figure S6 in SI). In other words, the precursor material is desorbed as expected for unreacted monomers. In UV-irradiated samples, the C1s signal remains constant even after 2 h of annealing above 400 °C, a temperature much higher than the sublimation temperature of 160 °C. This is the first evidence of the formation of higher-molecular weight compounds by UV irradiation. Notice that the C1s peaks after irradiation feature, if any, a shift toward the carbon sp^2 region (Figure S5 in SI) suggesting that the multilayers remain sp^2-hybridized within the limits of our experimental resolution (see SI). Figure 2c,f depicts the atomic force microscopy (AFM) images of the multilayer samples of **bba** and **dbba** after irradiation and annealing to 300 °C. A striking difference is obvious when comparing the samples in Figure 2c,f. For the UV-irradiated **dbba**, highly oriented elongated rods with mean thickness of 3 nm and longer than 50 nm are easily distinguished (Figure 2f). These are assigned to ribbon-like architectures of reacted monomers. It is also interesting that such UV-irradiated-annealed samples show long-range order, in contrast to the untreated samples (Figure S10 in SI).

To provide insight into the C–C coupling after or during C–Br photodissociation, we performed DFT-based transition-state calculations to find reaction and oligomerization mechanisms. Figure 3a,b depicts the coupled sp^2 multilayer

dx.doi.org/10.1021/ja412868w | J. Am. Chem. Soc. 2014, 136, 4651–4658

fabrication as a two-step reaction. First, the bromine is dissociated with an overall barrier of 3.83 eV (Figure 3a). Second, the reactivity of an aryl radical with an anthracene (Figure 3b) proceeds in a barrier-less manner, breaking aromaticity through an sp^3 carbon in the intermediate product (**IntS**). In a third step, dehydrogenation could occur, with a barrier for regaining aromaticity of 1.45 eV. This last step demonstrates that, even in the absence of a reducing agent, thermally removing monatomic hydrogen is possible. Figure 3c depicts an alternate concerted face-on bimolecular reaction pathway, showing that the halogenated carbon, in the vicinity of another one, will react to an intermediate state (**IntS$_1$**) with a barrier of 2.31 eV with respect to the ground state (**IS**). During this **IntS$_1$** step the C−Br distance changes from 1.92 Å to 2.06 Å, and a new C−C bond (1.63 Å) is formed. In a subsequent step, the anthracene rehybridizes to two C−C sp^2 carbons (1.46 Å) where the bromines leave (the Br−Br bond changes from 3.28 Å in the intermediate state to 2.32 Å). The final state (**FS**) is then recovered with a 30% reduced overall barrier than the nonconcerted mechanism. An extensive study of a bimolecular photoreaction pathway with TD-DFT is beyond the scope of the current study. However, the concerted mechanism put forward in Figure 3c is of arresting importance in solid-state photochemistry, as it suggests that only a C−Br 0.14 Å distance change suffices to react two neighboring anthracenes. A bimolecular pathway might also help explain why photodissociation proceeds faster in doubly brominated **dbba** than in single-brominated **bba** (Figure 2). Further investigation of such pathways might help to boost reaction selectivity in the solid-state.

Our LDI, XPS studies, and theoretical analysis aimed at an atomistic understanding of the C−Br dissociation, C−C reaction intermediates, and their possible coupling mechanisms during UV irradiation of nanometer-thin multilayers. In order to characterize the final photoreacted multilayers, we performed ToF-SIMS and Raman investigations. Unlike LDI, the SIMS ionization mechanism involves desorption and ionization through Bi_3^+ cluster impact.[22] This implies that SIMS alone cannot provoke photoinduced C−Br dissociation and coupling. Thus, ToF-SIMS allows us to confirm the formation of final C−C coupled products under UV irradiation of large-area samples. Figure 4a depicts the SIMS-ToF spectrum of the pristine **bba** on a gold substrate, showing the $[C_{28}H_{17}Br]^+$ isotopic pattern at 432 m/z. As expected, no tetraanthrylene (**ta**) oligomer signal $[C_{56}H_{34}]^+$ at 706 m/z is observed (Figure 4b). Notice that this last spectrum was acquired on a conductive substrate (Au/mica) in order to avoid the use of an electron flood gun to compensate for surface charging during measurement. In fact, when measuring the as-evaporated **dbba** on muscovite mica using a 21 eV flood gun, brominated n = 2 and n = 3 oligomers are observed (Figure 4c,d and Figure S11 in SI). These reactions are electron-induced, since neither brominated adducts nor tethraanthrylenes (Figure 4b) are detected in **dbba** SIMS studies on gold without the use of a 21 eV electron flood gun. Further inspection of the mass spectra in Figure 4c reveals a peak at 941 m/z, higher in intensity than the n = 2 dibrominated oligomer. As for the LDI in Figure 1a, this peak is identified as the triple brominated oligomer $[C_{56}H_{32}Br_3]^+$ (cf. Figure S11 in SI). As previously discussed, triple brominated adducts are possible if radicals further react with unreacted dibrominated precursors (via addition to anthracene moieties as indicated in Figure 3b). Consequently, the electron-induced process also provokes heterolytic dissociation of the C−Br bond. This unexpected result suggests that low-energy electrons might also be employed to "click" ordered π-stacked assemblies of brominated aromatic precursors via the face-on concerted mechanism described in Figure 3c.

With the possibility of electron-induced reactions in mind, the UV-irradiated and annealed multilayers shown in Figure 2c,f were characterized (Figure 4e−h). In such 300 °C annealed multilayers, electron-induced reactions are unequivocally avoided because thermal treatment removes any bromine that remains after UV irradiation (cf. Figure 2d). In fact, no traces of brominated adducts are observed in Figure 4e−h. This is consistent with covalently bound bromine having left the multilayer under UHV conditions. Figure 4e,f depict the SIMS data for the **bba** samples. As expected, they show as a major product above 400 m/z, a mixture of the **ta** species $[C_{56}H_{34}]^+ - 2H$ and $[C_{56}H_{34}]^+ - 1H$ (704 and 705 m/z, respectively) following the photoreaction. Because trianthrylene fragments are not observed, we assign the previous signals to ionization of intact rearomatized (−2H) **ta′** or deprotonated **ta** molecules. For the UV irradiation of **dbba**, the n = 2 $[C_{56}H_{33}]^+$ oligomers are also detected, albeit in smaller quantities (Figure 4g,h). It is noteworthy that SIMS-ToF analysis of **dbba** graphitized samples (*vide infra*) did not reveal the presence of monomers or dimers. Both observations are consistent with SIMS-ToF detecting only low-molecular weight polyaromatic compounds, which in turn indicate a higher degree of C−C coupling in **dbba** precursors as compared with **bba**.

Finally, the dehydrogenation step transforming the coupled sp^2-carbon multilayers into graphitic ones is of particular technological importance. Thus, Raman microspectroscopy (RM) measurements were performed for samples prepared on top of silicon oxide on silicon wafers. Unlike muscovite mica, silicon wafers can be used to record a RM signal. By using e-beam thermal-annealing (180 min, positive biasing the sample and using 10 mA cm^{-2} electron fluxes) to treat the C−C coupled multilayers, graphitic modes (D at 1330 cm^{-1} and G at 1595 cm^{-1}) are clearly observed (Figure 4i black line). While e-beam cross-linking of aromatic monolayers is a well-known process,[23] the overall strategy presented here is to use e-beam thermal treatment to provoke the final graphitization step of the (nano)architectures. This represents an increased level of molecular control provided by chemical design, photochemistry, and in situ mass spectrometry (cf. Scheme 1c−f). In fact, the Raman signatures obtained in Figure 4 are typical for polycrystalline graphene pyrolyzed on gold at 1000 °C[24] and pyrolyzed on copper at 700 °C.[25] The lower temperature for which we achieved similar results suggests that there is a reduced barrier for dehydrogenation of our coupled sp^2-carbon multilayers, tentatively due to cooperative dehydrogenation between anthracene units, as suggested previously.[26] Samples annealed at ∼500 °C without e-beam treatment also featured graphitization to some extent: In Figure 4i (red line) the sharp mode at 1445 cm^{-1} indicates remaining carbon sp^2 material. Note that higher temperatures were not attempted to avoid decomposition of SiO_x and mica. Unlike the aforementioned examples of (polycrystalline) graphene, all samples annealed at 500 °C (with and without e-beam treatment) showed reproducible Raman 2D peaks at ∼2920 cm^{-1}, 2745 cm^{-1}, and 2545 cm^{-1} (see Figure S12 in SI). Such articulated features are not present in disordered and damaged graphitic materials[27] and are indications of nanostructured polyaromatic compounds.[28]

dx.doi.org/10.1021/ja412868w | J. Am. Chem. Soc. 2014, 136, 4651−4658

CONCLUSIONS

In summary, UV irradiation of brominated aromatic precursors readily produces covalently coupled sp^2-carbon multilayers in which oligoanthracenes can be detected. Such coupled sp^2-carbon multilayers undergo graphitization already at 500 °C. We have provided insight into the photochemical and C−C coupling mechanisms via (TD-) DFT, consistent with XPS experiments and MS measurements. In doing so, we have introduced the field of photoinduced thin-film solid-state reactions as a convergence between top-down and selective bottom-up nanofabrication. We foresee that in-depth physicochemical control of nanometer-thin layered (self-)assembly along with the respective photochemical reaction mechanisms will provide a prosperous approach for directly patterning atomically precise graphene macromolecules and ribbons on insulating substrates. This is regarded as a useful and versatile strategy toward complex and extended carbon sp^2 macromolecules on insulators, thereby consolidating electronic/spintronic macromolecular blueprinting and engineering as a technological standard.

EXPERIMENTAL SECTION

Sample Preparation. For all experiments except when noted otherwise, samples were prepared under a base pressure in the 10^{-9} -10^{-10} mbar regime. Prior to molecule deposition by MBE, *ex situ* cleaved muscovite mica substrates were annealed to 300 °C to remove light contaminants, followed by a deposition of the **dbba** and **bba** molecules using organic MBE at a molecular temperature of 150−160 °C for 90 and 20 min, respectively, onto the muscovite mica which was kept at room temperature (RT). The films were measured to have a thickness close to 2 nm by AFM. Synthesis of **dbba** and **bba** molecules was carried out as described elsewhere[29] and products were triply sublimated before experiments to ensure high purity.

Time-of-Flight Laser Desorption Ionization. ToF-LDI and ToF-MALDI experiments were carried out in a Bruker FLEX2 spectrometers at a baser pressure of 10^{-6} mbar and a 7-ns pulsed Nitrogen Laser (337 nm). **Dbba** multilayers were fixed to a stainless steel target and the ions accelerated under a 15 kV field. The spectra collected belongs to single laser pulsing signal without averaging. MALDI experiments differed from ToF experiments in that a TCNQ matrix was sublimated on top of the **dbba** multilayers.

Time-Dependent Density Functional Theory. TD-DFT calculations, were performed using the Grid-based realspace Projector Augmented Wave function (GPAW) code, employing the Perdew, Burke, Ernzerhof (PBE) generalized gradient approximation for the exchange-correlation (xc)-functional.[30] Calculations for the isolated $C_{14}H_8Br$ and C_6H_5Br molecules were performed with more than 6 Å of vacuum surrounding the molecules and employing nonperiodic boundary conditions, forcing both the density and Kohn−Sham wave functions to go to zero at the boundaries of the unit cell. A commensurate grid spacing of h = 0.2 Å was employed throughout. In order to calculate the excitation energies of singlets and triplets, we first optimized the ground state geometries until all atomic Hellman-Feynman forces were below 0.05 eV/Å. We subsequently stretched the Br−C bond in steps of 0.1 Å, performing a further minimization of the geometry, while keeping the Br−C bond length fixed. In this way we determined the reaction coordinate for the Br dissociation reaction. For each relaxed geometry along the ground state dissociation reaction pathway we performed a separate TD-DFT calculation. From this we obtained both the singlet and triplet transitions, and their respective energies and oscillator strengths. The exact description of this procedure is given in the SI.

Density Functional Theory. DFT calculations for the reaction pathways were carried out with the VASP code.[31] A variant of the van der Waals density functional[32] was used, with the exchange replaced by an optimized form of the Becke 86 exchange functional.[33] The plane waves were expanded to a cutoff of 400 eV and the Γ-point was used to sample the first Brillouin zone. Energy barriers were obtained by transition state calculations following the approach described in ref.[26] using a combination of the climbing image nudged elastic band[34] (CI-NEB) and dimer[35] methods. In short, CI-NEB was used to find an initial estimate of the transition state. The estimate was then used to generate the input (central image and dimer) in the dimer method. Structural optimizations of both local minima and transition states were performed until the residual forces were smaller than 0.02 eV/Å.

X-ray Photoelectron Spectroscopy. The XPS experiments were performed in an UHV chamber with a base pressure in the 10^{-9} -10^{-10} mbar regime. A nonmonochromatized Mg Kα X-ray source ($h\nu$ = 1253.6 eV) was used for the XPS measurements which were conducted at RT. The data were obtained using a hemispherical electron energy analyzer (100 mm radius) operated at a pass energy of 20 eV. The analyzer was equipped with a position sensitive resistive anode detector for increased sensitivity. Due to the sensitivity of the molecules to electrons, the measurements were performed without the use of a flood gun, resulting in a shift of approximately 3.5 eV to higher binding energies due to charging. This shift was corrected by referencing all spectra to the mica Al2p peak at 74.4 eV[36] (for further information see SI). Afterward a linear (Br3d), constant (C1s, dbba) or a Shirley (C1s, bba) background was subtracted. Note that the magnesium X-ray source and/or the occurrence of secondary electrons during XPS measurements also induce (high-energy) C−Br photodissociation, as evidenced by reduction of the Br 3d peak (see Figure S8 in SI). This effect seems to be much more prominent for **bba** than for **dbba**. Our experiments indicate that for **bba** it takes 320 min of continuous X-ray exposure to produce the same effect as 180 min of UV irradiation. Therefore the experiments above were conducted such that the exposure to X-ray irradiation was minimal and the spectra of two subsequent measurements did not show any substantial difference (see Figure S8 in SI).

Time-of-Flight Secondary Ion Mass Spectrometry. ToF-SIMS was performed on a TOF.SIMS5 instrument (ION-TOF GmbH, Münster, Germany), equipped with a Bi cluster primary ion source and a reflectron type time-of-flight analyzer. UHV base pressure was $<5 \times 10^{-9}$ mbar. For high mass resolution the Bi source was operated in the "high current bunched" mode providing short Bi_1^+ or Bi_3^+ primary ion pulses at 25 keV energy and a lateral resolution of approximately 4 μm. The short pulse length of 1.1 to 1.3 ns allowed for high mass resolution. The primary ion beam was rastered across a 500 × 500 μm field of view on the sample, and 128 × 128 data points were recorded. Primary ion doses were kept below 10^{11} ions/cm^2 (static SIMS limit). Charge compensation was necessary because of the insulating samples so that an electron flood gun providing electrons of 21 eV was applied and the secondary ion reflectron tuned accordingly.

ASSOCIATED CONTENT

Supporting Information

Additional ToF-LDI, TD-DFT, XPS, AFM, Raman, ToF-SIMS experiments, and synthetic methods. This material is available free of charge via the Internet at http://pubs.acs.org.

AUTHOR INFORMATION

Corresponding Authors

*c.a.palma@tum.de
*florian.klappenberger@tum.de
*angel.rubio@ehu.es
*muellen@mpg.mpip-mainz.de

Notes

The authors declare no competing financial interest.

ACKNOWLEDGMENTS

The authors are especially grateful to Karl Eberle for XPS measurements and Thomas Schuster for additional LDI measurements. We gratefully acknowledge silicon wafers from Jose Antonio Garrido and preliminary Raman measurements

from Max Seifert, Stefan Funk, Stefan Niedermayer, and Hai Bi. C.-A.P. thanks Hristo Iglev for continuous help, Christian Lütke-Eversloh for additional UV data and Achim Hartschuh for support. We acknowledge financial support from the European Research Council Advanced Grant DYNamo (ERC-2010-AdG-267374) Spanish Grants (FIS2010-21282-C02-01 and PIB2010US-00652), Grupos Consolidados UPV/EHU del Gobierno Vasco (IT578-13), Ikerbasque and the European Commission projects CRONOS (Grant 280879-2 CRONOS CP-FP7). C.-A.P. and K.D. were funded through the ERC Advanced Grant MolArt (no. 247299). D.J.M. acknowledges funding through the Spanish "Juan de la Cireva" program (JCI-2010-08156). J.L.C acknowledges funding through the Mexican CONACyT program. J.B. acknowledges the National Supercomputer Centre, Sweden, for computational resources.

REFERENCES

(1) Grill, L.; Dyer, M.; Lafferentz, L.; Persson, M.; Peters, M. V.; Hecht, S. *Nat. Nanotechnol.* **2007**, *2*, 687.
(2) Palma, C. A.; Samorì, P. *Nat. Chem.* **2011**, *3*, 431.
(3) (a) Abel, M.; Clair, S.; Ourdjini, O.; Mossoyan, M.; Porte, L. *J. Am. Chem. Soc.* **2011**, *133*, 1203. (b) Bieri, M.; Treier, M.; Cai, J. M.; Ait-Mansour, K.; Ruffieux, P.; Gröning, O.; Gröning, P.; Kastler, M.; Rieger, R.; Feng, X. L.; Müllen, K.; Fasel, R. *Chem. Commun.* **2009**, 6919.
(4) Cai, J. M.; Ruffieux, P.; Jaafar, R.; Bieri, M.; Braun, T.; Blankenburg, S.; Muoth, M.; Seitsonen, A. P.; Saleh, M.; Feng, X. L.; Müllen, K.; Fasel, R. *Nature* **2010**, *466*, 470.
(5) Zhang, Y. Q.; Kepčija, N.; Kleinschrodt, M.; Diller, K.; Fischer, S.; Papageorgiou, A. C.; Allegretti, F.; Björk, J.; Klyatskaya, S.; Klappenberger, F.; Ruben, M.; Barth, J. V. *Nat. Commun.* **2012**, *3*, 549.
(6) McNaught, A. D.; Wilkinson, A. *IUPAC Compendium of Chemical Terminology*, 2nd ed.; International Union of Pure and Applied Chemistry (IUPAC): London, **1997**.
(7) (a) Björk, J.; Hanke, F.; Stäfstrom, S. *J. Am. Chem. Soc.* **2013**, *135*, 5768. (b) Ertl, G. *Reactions at Solid Surfaces*; John Wiley & Sons, Inc.: Hoboken, NJ, 2009. (c) Zhong, D. Y.; Franke, J. H.; Podiyanachari, S. K.; Blömker, T.; Zhang, H. M.; Kehr, G.; Erker, G.; Fuchs, H.; Chi, L. F. *Science* **2011**, *334*, 213.
(8) (a) Kittelmann, M.; Nimmrich, M.; Lindner, R.; Gourdon, A.; Kühnle, A. *ACS Nano* **2013**, *7*, 5614. (b) Bombis, C.; Ample, F.; Lafferentz, L.; Yu, H.; Hecht, S.; Joachim, C.; Grill, L. *Angew. Chem., Int. Ed.* **2009**, *48*, 9966. (c) Gutzler, R.; Walch, H.; Eder, G.; Kloft, S.; Heckl, W. M.; Lackinger, M. *Chem. Commun.* **2009**, 4456.
(9) Sloan, D.; Sun, Y. M.; Ihm, H.; White, J. M. *J. Phys. Chem. C.* **1998**, *102*, 6825.
(10) Bieri, M.; Nguyen, M. T.; Gröning, O.; Cai, J. M.; Treier, M.; Ait-Mansour, K.; Ruffieux, P.; Pignedoli, C. A.; Passerone, D.; Kastler, M.; Müllen, K.; Fasel, R. *J. Am. Chem. Soc.* **2010**, *132*, 16669.
(11) Colson, J. W.; Dichtel, W. R. *Nat. Chem.* **2013**, *5*, 453.
(12) (a) Han, K. L.; He, G. Z. *J. Photochem. Photobiol., C* **2007**, *8*, 55. (b) Davidson, R. S.; Goodin, J. W.; Kemp, G. *Adv. Phys. Org. Chem.* **1984**, *20*, 191. (c) Kadi, M.; Davidsson, J.; Tarnovsky, A. N.; Rasmusson, M.; Akesson, E. *Chem. Phys. Lett.* **2001**, *350*, 93.
(13) Szulczewski, G. J.; White, J. M. *Surf. Sci.* **1998**, *399*, 305.
(14) Bouas-Laurent, H.; Castellan, A.; Desvergne, J. P.; Lapouyade, R. *Chem. Soc. Rev.* **2000**, *29*, 43.
(15) Chen, S. F.; Liu, F. Y.; Liu, Y. J. *J. Chem. Phys.* **2009**, 131.
(16) Mcgimpsey, W. G.; Scaiano, J. C. *J. Am. Chem. Soc.* **1989**, *111*, 335.
(17) Pijpers, A. P.; Meier, R. J. *J. Electron Spectrosc. Relat. Phenom.* **2001**, *121*, 299.
(18) Hunger, R.; Jaegermann, W.; Merson, A.; Shapira, Y.; Pettenkofer, C.; Rappich, J. *J. Phys. Chem. B.* **2006**, *110*, 15432.
(19) Thompson, A.; Attwood, D.; Gullikson, E.; Howells, M.; Kim, K.-J.; Kirz, J.; Kortright, J.; Lindau, I.; Liu, Y.; Pianetta, P.; Robinson, A.; Scofield, J.; Underwood, J.; Wiliams, G. *X-ray Data Booklet Lawrence Berkeley National Laboratory*; University of California: Berkeley, CA, 2009.
(20) Yeh, J. J.; Lindau, I. *At. Data Nucl. Data Tables* **1985**, *32*, 1.
(21) Knochenmuss, R.; Zenobi, R. *Chem. Rev.* **2003**, *103*, 441.
(22) Kollmer, F. *Appl. Surf. Sci.* **2004**, *231*, 153.
(23) Geyer, W.; Stadler, V.; Eck, W.; Zharnikov, M.; Gölzhäuser, A.; Grunze, M. *Appl. Phys. Lett.* **1999**, *75*, 2401.
(24) Turchanin, A.; Weber, D.; Buenfeld, M.; Kisielowski, C.; Fistul, M. V.; Efetov, K. B.; Weimann, T.; Stosch, R.; Mayer, J.; Gölzhäuser, A. *ACS Nano* **2011**, *5*, 3896.
(25) Matei, D. G.; Weber, N.-E.; Kurasch, S.; Wundrack, S.; Woszczyna, M.; Grothe, M.; Weimann, T.; Ahlers, F.; Stosch, R.; Kaiser, U.; Turchanin, A. *Adv. Mater.* **2013**, *25*, 4146.
(26) Björk, J.; Stafström, S.; Hanke, F. *J. Am. Chem. Soc.* **2011**, *133*, 14884.
(27) Pimenta, M. A.; Dresselhaus, G.; Dresselhaus, M. S.; Cancado, L. G.; Jorio, A.; Saito, R. *Phys. Chem. Chem. Phys.* **2007**, *9*, 1276.
(28) (a) Huang, H.; Wei, D. C.; Sun, J. T.; Wong, S. L.; Feng, Y. P.; Neto, A. H. C.; Wee, A. T. S. *Sci. Rep.* **2012**, *2*, 983. (b) Dössel, L.; Gherghel, L.; Feng, X. L.; Müllen, K. *Angew. Chem., Int. Ed.* **2011**, *50*, 2540.
(29) Müller, U.; Baumgarten, M. *J. Am. Chem. Soc.* **1995**, *117*, 5840.
(30) Perdew, J. P.; Burke, K.; Wang, Y. *Phys. Rev. B* **1996**, *54*, 16533.
(31) Kresse, G.; Furthmüller, J. *Phys. Rev. B* **1996**, *54*, 11169.
(32) Dion, M.; Rydberg, H.; Schröder, E.; Langreth, D. C.; Lundqvist, B. I. *Phys. Rev. Lett.* **2004**, 92.
(33) Klimeš, J.; Bowler, D. R.; Michaelides, A. *J. Phys. Condens. Matter* **2010**, *22*, 022201.
(34) Henkelman, G.; Uberuaga, B. P.; Jonsson, H. *J. Chem. Phys.* **2000**, *113*, 9901.
(35) (a) Henkelman, G.; Jonsson, H. *J. Chem. Phys.* **1999**, *111*, 7010. (b) Kaestner, J.; Sherwood, P. *J. Chem. Phys.* **2008**, 128.
(36) Bhattacharyya, K. G. *J. Electron Spectrosc. Relat. Phenom.* **1993**, *63*, 289.